Inclusion compounds of binaphthol with xylidines: structures, selectivity and kinetics of desolvation

Luigi R. Nassimbeni * and Hong Su

Department of Chemistry, University of Cape Town, Rondebosch 7701, South Africa

Received (in Cambridge, UK) 6th December 2001, Accepted 30th April 2002
First published as an Advance Article on the web 31st May 2002

The inclusion compounds of binaphthol with three isomers of xylidine have been studied in terms of their structures and infra-red spectra. Competition experiments show that the selectivity of enclathration follows the trend: 2,6-xylidine > 2,3-xylidine ≈ 3,5-xylidine. The kinetics of desolvation have been analysed and the activation energies established.

Introduction

The formation and stability of a particular inclusion compound depend on the strengths and directions of the intermolecular forces which act on the host–guest system. Therefore accurate structure determination by single crystal X-ray diffraction is an important tool, in that it yields not only detailed structural parameters of the individual host and guest molecules, but it also affords a description of their packing. Thus it is possible to describe the topology of space in which the guests are encapsulated, which in turn impinges on the macro properties of the inclusion compound, such as its thermal stability, its guest selectivity, its ability to withstand guest exchange and its kinetics of formation and decomposition.

The process of selective enclathration has been studied in a varity of host–guest systems. α-Cyclodextrin and urea have been employed to separate mixtures of poly(ethylene glycol)s of different molecular weights.[1] Substituted resorcinarenes and calixarenes have been used to separate aromatic hydrocarbons.[2] *N*,*N*′-Ditritylurea and a range of analogs have been synthesised and their clathrating properties and selectivity with a variety of aliphatic guests have been established.[3] The inclusion properties of 1,4-(triorganostannyl and silyl)buta-1,3-diyne with chlorinated solvents and simple aromatic molecules have been studied.[4] These hosts mimic the noted Toda host 1,1,6,6-tetraphenylhexa-2,4-diyne-1,6-diol which has been studied extensively and has been employed in the separation of close isomers.[5–7] Gas chromatographic techniques are particularly useful in the study of guest selectivity, and these have been recently applied to test the inclusion preference of *p*-*tert*-butylcalix[4]arene and *p*-*tert*-butylcalix[8]arene towards positional isomers of xylenes, ethyltoluenes and diethylbenzenes.[8] We now present the results of the structural analyses, thermal stability, desorption kinetics and guest selectivity of the host 2,2′-dihydroxy-1,1′-binaphthyl (binaphthol, **BNP**) with three isomers of xylidine. The atomic numbering scheme is shown in Scheme 1.

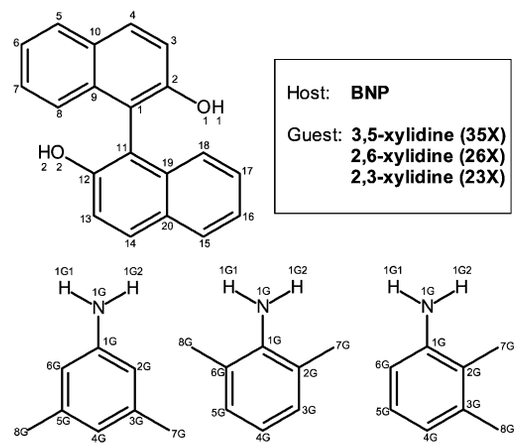

Scheme 1

Results and discussion

Crystal structure †

Suitable single crystals of the inclusion compounds were obtained by dissolving the host in the liquid xylidines and allowing slow concentration over a period of 7 days at room temperature. Details of the crystal data, data collections and refinement are given in Table 1. Cell dimensions were established from the intensity data measurements in a Nonius Kappa CCD diffractometer using graphite-monochromated Mo-Kα radiation. The strategy for the data collections was evaluated using the COLLECT[9] software. For all three structures data were collected by the standard phi scan and omega scan techniques and were scaled and reduced using DENZO-SMN[10] software. The structures were solved by direct methods using SHELX-86[11] and refined by full-matrix least-squares with SHELX-97[12] refining on F^2. The program X-Seed[13] was used as a graphical interface for structure solution and refinement using SHELX.

BNP·35X crystallises in $P\bar{1}$ with $Z = 2$, so both host and guest molecules are placed in general positions. The hydroxy hydrogens of the host and the amino hydrogens of the guest were located in difference electron density maps and refined with simple bond length constraints. The packing is displayed in Fig. 1a, which shows the structure is stabilised by a (host)O–H ··· N(guest) hydrogen bond. The metrics of the hydrogen bonding for this and the other two compounds are given in Table 2. The 3,5-xylidine guests lie in channels running parallel to [100], as shown in Fig. 2.

BNP·2(26X) crystallises in *C*2/*c* with $Z = 4$. The host therefore lies at a special position on the diad at Wyckoff position *e* and the guest is located in a general position. The host hydroxy hydrogen was found and refined as before, but the guest amino hydrogens could not be located and were omitted from the final

† CCDC reference numbers 176345–176347. See http://www.rsc.org/suppdata/p2/b2/b204190c/ for crystallographic files in .cif or other electronic format.

 DOI: 10.1039/b204190c

Table 1 Details for crystal data, data collection and refinement

Inclusion compound	**BNP·35X**	**BNP·2(26X)**	**BNP·3(23X)**
Molecular formula	$C_{20}H_{14}O_2 \cdot C_8H_{11}N$	$C_{20}H_{14}O_2 \cdot 2C_8H_{11}N$	$C_{20}H_{14}O_2 \cdot 3C_8H_{11}N$
Formula weight/g mol^{-1}	407.49	528.67	649.85
Crystal system	Triclinic	Monoclinic	Orthorhombic
Space group	$P\bar{1}$	$C2/c$	$Pbca$
a/Å	8.907(2)	26.066(2)	22.634(1)
b/Å	8.956(3)	10.068(2)	10.464(1)
c/Å	13.887(2)	11.868(2)	30.689(1)
α/°	98.68(2)	90	90
β/°	98.45(1)	109.11(5)	90
γ/°	94.26(2)	90	90
Volume/Å^3	1077.9(5)	2943.0(8)	7268.4(8)
Z	2	4	8
D_c/g cm^{-3}	1.255	1.193	1.188
F(000)	432	1128	2784
μ/mm^{-1}	0.078	0.073	0.073
Range scanned, θ/°	2.31–24.97	1.65–24.97	1.60–24.66
Temperature/K	253	293	173
No. of measured reflections	4042	5323	24311
No. of independent reflections	3787	2574	5926
No. of observed reflections	2615	1791	3329
R_{int}	0.0243	0.0259	0.0721
Range of indices, h, k, l	±10/±10/0,16	−30,11/±11/−13,14	−19,26/−9,11/−33,36
Final R indices [$F_o > 4(F_o)$], $R1$	0.0401	0.0662	0.0926
$wR2$ (F^2)	0.1096	0.1960	0.2539
R indices (all data)	0.0740	0.1006	0.1879
Goodness of fit on F^2, S	1.034	1.068	1.040
Weighting scheme	$w =$	$w =$	$w =$
{where $P = [\mathrm{Max.}(F_o^2,0) + 2F_c^2]/3$}	$1/[\sigma^2(F_o^2) + (0.061P)^2 + 0.15P]$	$1/[\sigma^2(F_o^2) + (0.12P)^2 + 2.18P]$	$1/[\sigma^2(F_o^2) + (0.15P)^2 + 7.44P]$
Max./min. height $\Delta\rho$ in difference electron map/e Å^{-3}	0.180/−0.166	0.602/−0.256	0.968/−0.411
Extinction coefficient	0.020(3)	0.0014(10)	0.0012(5)

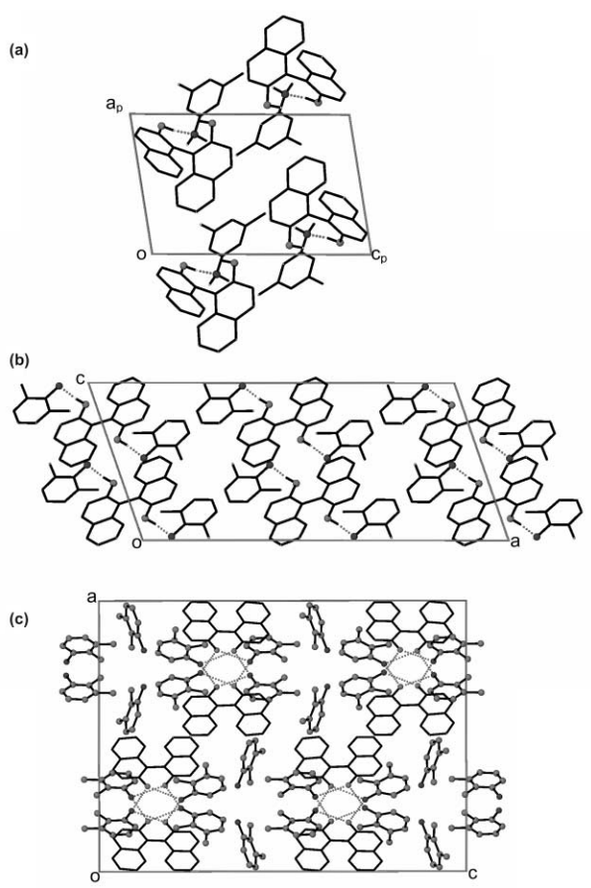

Fig. 1 Packing diagrams viewed along [010] for compounds **BNP·35X**, **BNP·2(26X)** and **BNP·3(23X)** in (a), (b) and (c) respectively. Only the hydroxy and amino hydrogens are shown in (a) and only the hydroxy hydrogens are shown in (b). All hydrogens are omitted in (c). H-bonds are indicated as dotted lines.

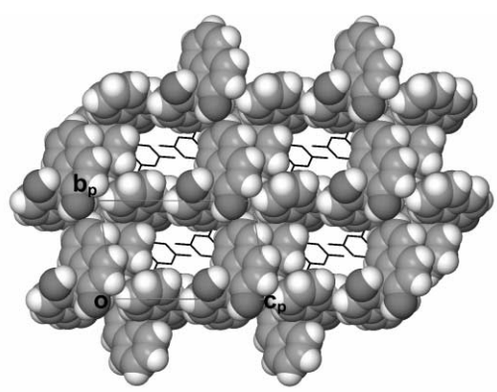

Fig. 2 Projection down [100] showing the top of the open channels in the structure of **BNP·35X**. The host molecules are shown with van der Waals radii and the guest molecules are shown in a stick representation.

model. A (host)O–H ··· N(guest) hydrogen bond is present (Table 2) and the 2,6-xylidine molecules are located in channels running in the [110] and [1$\bar{1}$0] directions at z = 1/4 and 3/4. These are shown in Fig. 3. The packing projected down [010] is shown in Fig. 1b.

BNP·3(23X) crystallises in *Pbca* with Z = 8. All host and guest molecules are in general positions. All hydroxy and amino hydrogens were located in difference electron density maps and were refined with simple bond length constraints. The structure exhibits extensive hydrogen bonding, the host hydroxy and the guest amino groups act as both proton donors and acceptors. There are three independent guest molecules, one of which is not hydrogen bonded, while the other two act as double bridges linking adjacent host molecules chaining along [010]. A projection of the structure is shown in Fig. 1c. The guests are located in crossing channels running parallel to [010] and [001].

IR spectra were recorded for the apohost **BNP** as well as the three inclusion compounds in the region of the hydroxy stretching frequency (3000–3600 cm^{-1}). The crystal structure of the

Table 2 Hydrogen bonding details for all the structures and results from IR spectra

Compounds	D–H ··· A[a]/Å	H ··· A/Å	D ··· A/Å	<DHA/°	ν_{OH}/cm^{-1}	$\Delta = \nu_f - \nu_{OH}$
BNP[14]	O(1)–H(1) ··· O(2)[1]	2.03	2.852	141	3398.7	85
					3483.7 (ν_f)	/
BNP·35X	O(1)–H(1) ··· N(1G)	1.91(1)	2.837(2)	163(2)	3318.6	165.1
					3388.3	95.4
BNP·2(26X)	O(1)–H(1) ··· N(1G)	1.86(1)	2.814(3)	171(3)	3311.2	172.5
BNP·3(23X)	O(1)–H(1) ··· N(1GA)[2]	1.82(2)	2.767(5)	164(4)	3370.8	112.9
	O(2)–H(2) ··· N(1GB)[3]	1.80(2)	2.735(5)	163(4)	3281.3	202.4
	N(1GA)–H(1A1) ··· O(2)	2.12(2)	3.041(5)	158(4)		
	N(1GB)–H(1B1) ··· O(1)	2.09(2)	2.984(5)	155(4)		

[a] **D–H ··· A**: Donor (**D**)–**H** ··· Acceptor (**A**). Symmetry codes: (1) $-x + 1/2, -y + 1/2, z - 1/2$; (2) $-x + 1/2, y - 1/2, z$; (3) $-x + 1/2, y + 1/2, z$.

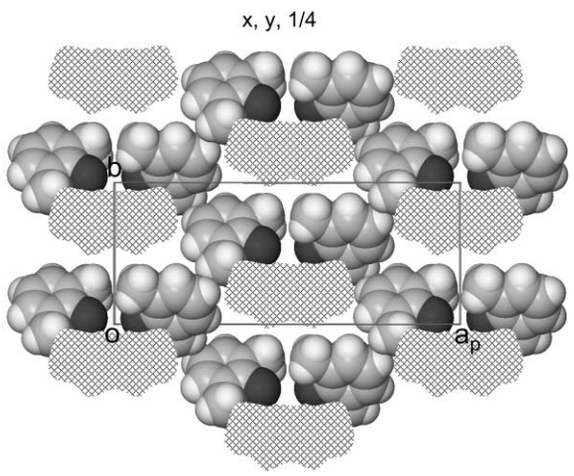

Fig. 3 Projected cross section on (004) showing the guest molecules located in cross running channels in the structure of **BNP·2(26X)**. The grey areas represent the space occupied by the host.

apohost shows that only one of the two hydroxy groups is hydrogen bonded.[14] Its IR spectra displayed two sharp peaks, at 3483.7 cm^{-1} which we attribute to the 'free' O–H and at 3398.7 cm^{-1} due to the hydrogen bonded hydroxy [d(O–H ··· N) = 2.839 Å]. We have noted that in all cases the recorded IR bonds occur at lower frequencies, and the frequency changes $\Delta = \nu_f - \nu_{OH}$ are recorded in Table 2, together with the details of the hydrogen bonding observed in their crystal structures. The case of **BNP·35X** merits special mention, in that only one host hydroxy is hydrogen bonded with (host)O–H ··· N(guest) having d(O ··· N) = 2.837 Å and Δ = 165.1 cm^{-1}, but the other O–H has a close contact with a methyl group from the 3,5-xylidine with (host)O–H ··· CH_3(guest) having d(H ··· C) = 2.763 Å, resulting in a vibrational shift of 95.4 cm^{-1}.

The torsion angle C(2)–C(1)–C(11)–C(12), which defines the conformation of the host, varies from 75.9(4)° in **BNP·2(26X)** through 88.3(2)° in **BNP·35X** to 94.8(5)° in **BNP·3(23X)**. This fairly wide range shows that the two binaphthyl ring systems are relatively flexible and can twist with respect to each other in order to accommodate guest molecules of different size and geometry. A search of the Cambridge Structural Database System[15] yields 39 entries for this host molecule, with this torsion angle varying from 69° to 109°, and averaging 90°.

Competition experiments

These were carried out in solutions as follows. A series of 9 vials was made up with mixtures of two guests such that the mole fraction of a given guest varied from 0 to 1. The host was added to each mixture keeping the ratio of total guest to host at about 15 : 1 and dissolved by warming. The vials were left open at room temperature and the resulting crystalline inclusion compounds were filtered, dried and dissolved in chloroform and these, as well as the mother liquors, were analysed by gas chromatography. The results are shown in Fig. 4a, b and c, in which X represents the mole fraction of a given guest in the liquid mixture, and Z the mole fraction of that guest in the crystals. The diagonal line represents zero selectivity. The results show that 2,6-xylidine is preferentially enclathrated over both 3,5-xylidine and 2,3-xylidine over practically the whole range of mixtures, while Fig. 4c shows that there is virtually zero selectivity between 3,5-xylidine and 2,3-xylidine. The experiment was extended to analyse simultaneous competition by all three isomers. The results are shown in Fig. 4d, where the apices of the equilateral triangle represent pure isomers. Starting mixtures are represented by a point and the results of the inclusion are shown by arrows. These show that 2,6-xylidine is strongly favoured when its starting mole fraction $X_{26X} > 0.2$, otherwise 2,3-xylidine and 3,5-xylidine are equally selected. The three component competition results are in good agreement with those observed from the two-component competitions.

Thermal analysis

Thermogravimetry (TG) and differential scanning calorimetry (DSC) were carried out on a Perkin-Elmer PC7-Series system. The experiments were performed over a temperature range of 30–230 °C at a constant heating rate of 10 °C min^{-1} with a purge of dry nitrogen flowing at 30 ml min^{-1}. The samples were crushed, blotted dry and placed in open platinum pans for TG experiments and in crimped but vented aluminium pans for DSC. The results of the TG are displayed in Fig. 5a, which shows that each compound undergoes a single step desolvation. The DSC results, shown in Fig. 5b, indicate a first endotherm due to guest release followed by a second endotherm attributed to the guest melt. Calculated and observed mass losses and onset temperatures for guest release (T_{on}), as well as the difference between T_{on} and the boiling point of pure guest (T_b) for each inclusion compound are given in Table 3.

Kinetics of desolvation

The data for the kinetics of desolvation were obtained by isothermal TG experiments on finely crushed microcrystalline samples of the inclusion compounds. The fraction decomposed, α, was calculated from the mass loss $\alpha = (m_o - m_t)/(m_t - m_f)$, where m_o is the initial mass, m_t is the mass at time t and m_f is the final mass. For **BNP·35X** and **BNP·2(26X)**, the *α–time* curves were deceleratory and were best described by the contracting area (R2) equation:[16]

$$1 - (1 - \alpha)^{1/2} = kt \quad (1)$$

Arrhenius parameters were obtained over an α range of 0.05 to 0.95 with coefficients between 0.993 and 0.999. Plots of ln k *vs.* $1/T$ are shown in Fig. 6, and yielded activation energies of 106(8) and 88(4) kJ mol^{-1} for **BNP·35X** and **BNP·2(26X)** respectively.

For the desolvation of **BNP·3(23X)**, the *α–time* curves were sigmoidal and fitted the A2 equation:[16]

$$[-\ln(1 - \alpha)]^{1/2} = kt \quad (2)$$

Table 3 Thermal analysis results for the inclusion compounds

Inclusion compounds	Observed weight loss from TG (%)	Calculated weight loss (%)	Guest release T_{on}/°C	Apohost melting T_m/°C	Bp of pure guest T_b/°C	$T_{on} - T_b$
BNP·35X	29.2	29.74	136.9	215.8	221	−84.1
BNP·2(26X)	44.5	45.84	110.9	215.1	214	−103.1
BNP·3(23X)	56.2	55.94	64.1	215.5	223	−158.9

Table 4 Kinetic parameters for the desolvations of the inclusion compounds

Inclusion compound	Temperature range/K	α range	Kinetic model	E_a/kJ mol^{-1}	ln A
BNP·35X	353–403	0.05–0.95	R2	106(8)	29(3)
BNP·2(26X)	343–403	0.05–0.95	R2	88(4)	24(1)
BNP·3(23X)	323–348	0.07–0.93	A2	108(8)	35(3)
	358–393	0.07–0.93	A2	59(5)	18(2)

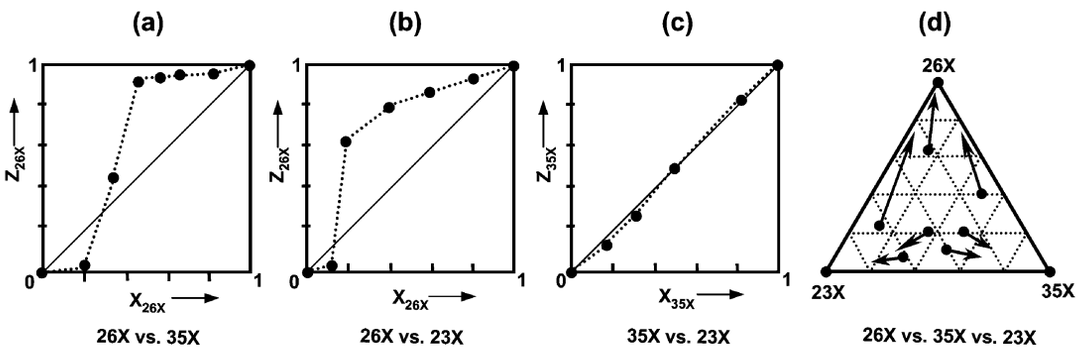

Fig. 4 Competition results.

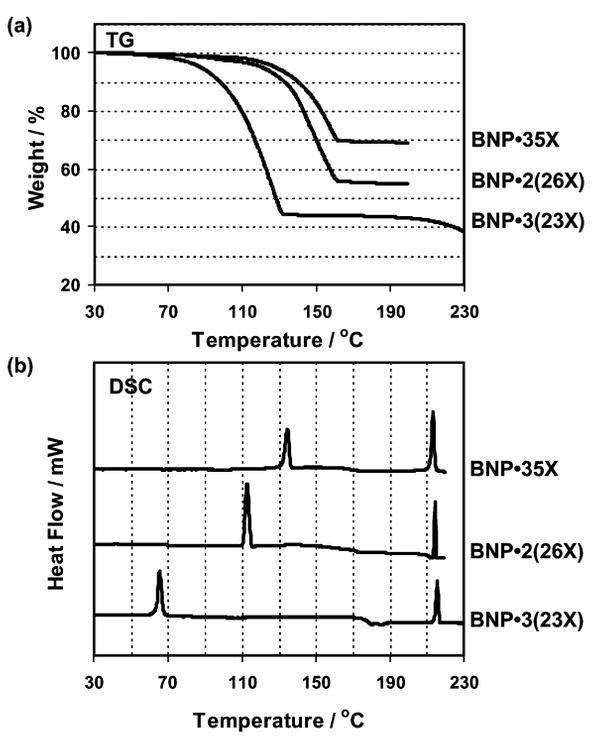

Fig. 5 Thermal analysis results: TG and DSC curves.

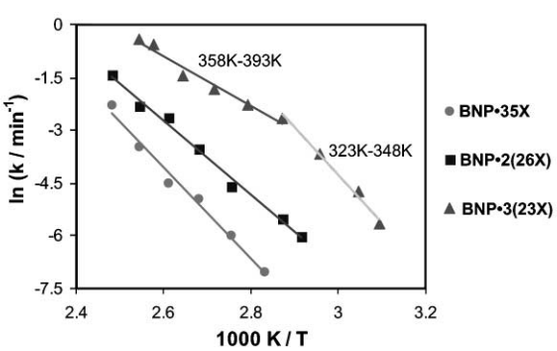

Fig. 6 Arrhenius plot of ln k *vs.* $1/T$.

The Arrhenius semi-logarithmic plot, however, is not linear over the complete temperature range of 323 to 393 K, but yields two distinct lines of differing slopes which cross at $1/T$ at 2.91×10^{-3} K^{-1} (T = 344 K), corresponding to two activation energies of 108(8) and 59(5) kJ mol^{-1}. This was initially puzzling, as the fit of the A2 rate equation was good over the entire temperature range. We therefore investigated the crystals by hot stage microscopy. This revealed that the crystals, which were initially transparent, developed cracks and became opaque in the temperature range 298 to 346 K, at which point liquid guest appeared and partly dissolved the crystals. By 350 K most of the liquid had disappeared, leaving opaque crystals which melted at 488 K. We surmise therefore that from 358 to 393 K the *α–time* curves represent a combination of desolvation and liquid solvent evaporation, yielding the lower activation energy. A summary of the kinetic parameters is given in Table 4.

Similar activation energies were obtained for the desolvation of the isomers of methylcyclohexanones from their inclusion compounds with *trans*-9,10-dihydroxy-9,10-diphenyl-9,10-dihydroanthracene.[17]

Conclusion

We have noted that with similar inclusion compounds formed between binaphthol and the isomers of picoline, the stoichiometries have a host : guest ratio of 1 : 2 for all three compounds. This allowed us to correlate their relative thermal stabilities in terms of $T_{on} - T_b$ with their lattice energies, and their selectivity results.[18] However this was not possible in this case where the host : guest ratios of binaphthol with

3,5-xylidine, 2,6-xylidine and 2,3-xylidine were 1 : 1, 1 : 2 and 1 : 3 respectively. Lattice energy values are dependent on the summation of atom-pair potentials, and are only comparable in cases where the stoichiometries are the same. Therefore, in this work, there is no direct correlation between the thermal stability and the selectivity results. We note, moreover, that in the structure of **BNP·3(23X)**, two of the guests are hydrogen bonded to the host and the third is not. In such a situation one sometimes observes different endotherms in the DSC with concomitant multiple steps in the TG.[19] This did not occur in our case, as the desorption of 2,3-xylidine occurred in one step in the TG, with a corresponding single endotherm in the DSC.

References

1 C. C. Rusa and A. E. Tonelli, *Macromolecules*, 2000, **33**, 1813.
2 V. I. Kalchenko, A. V. Solovov, N. R. Gladun, A. N. Shivanyuk, L. I. Atamas, V. V. Pirozhenko, L. N. Markovsky, J. Lipkowski and Y. A. Simonov, *Supramol. Chem.*, 1997, **8**, 269.
3 K. D. Ng and H. Hart, *Tetrahedron*, 1995, **51**, 7883.
4 F. Carré, S. G. Dutremez, C. Guériu, B. J. L. Henner, A. Jolivet, V. Tomberli and F. Dahan, *Organometallics*, 1999, **18**, 770.
5 J. Bacsa, M. R. Caira, A. Jacobs, L. R. Nassimbeni and F. Toda, *Cryst. Eng.*, 2000, **3**, 251.
6 M. R. Caira, L. R. Nassimbeni, F. Toda and D. Vujovic, *J. Chem. Soc., Perkin Trans. 2*, 2001, 2119.
7 M. R. Caira, L. R. Nassimbeni, F. Toda and D. Vujovic, *J. Am. Chem. Soc.*, 2000, **122**, 9367.
8 P. Mñuk, L. Feltl and V. Schuria, *J. Chromatogr., A.*, 1996, **732**, 63.
9 COLLECT, data collection software, Nonius, Delft, Netherlands, 1998.
10 Z. Otwinowski and W. Minor, in *Methods in Enzymology, Macromolecular Crystallography*, Part A, Vol. 276, eds. C. W. Carter, Jr. and R. M. Sweet, Academic Press, 1997, p. 307.
11 G. M. Sheldrick, SHELX-86, in Crystallographic Computing, eds. G. M. Sheldrick, C. Kruger and R. Goddard, Oxford University Press, Oxford, UK, 1985, **Vol. 3**, p. 175.
12 G. M. Sheldrick, SHELX-97: A Programme for Crystal Structure Determination, University of Göttingen, Germany, 1997.
13 L. J. Barbour, X-Seed: a graphical interface for the SHELX program, University of Missouri-Columbia, USA, 1999.
14 K. Mori, Y. Masuda and S. Kashino, *Acta Crystallogr., Sect. C*, 1993, **49**, 1224.
15 CSDS: Cambridge Structural Database System, Version 5.22, Cambridge Crystallographic Data Centre, Cambridge, UK, 2001.
16 M. E. Brown, in *Introduction to Thermal Analysis—Techniques and Applications*, Chapman and Hall, London, 1988, chapter 13.
17 A. Coetzee, L. R. Nassimbeni and H. Su, *J. Chem. Res.*, 1999, 436.
18 L. R. Nassimbeni and H. Su, *Acta Crystallogr., Sect. B.*, 2001, **57**, 394.
19 E. Weber, K. Skobridis, A. Wierig, L. J. Barbour, M. R. Caira and L. R. Nassimbeni, *Chem. Ber.*, 1993, **126**, 1141.